Correlation between the activation energies of structural relaxation and viscous flow for $BaO-P_2O_5-Al_2O_3$ glasses

Roman Svoboda*[a], Maria Chromčíková[b,c], Branislav Hruška[c], Marek Liška[b,c]

[a] *University of Pardubice, Faculty of Chemical Technology, Department of Physical Chemistry, Studentská 573, 532 10 Pardubice, Czech Republic*
[b] *Institute of Inorganic Chemistry of Slovak Academy of Sciences, Bratislava, Dúbravská cesta 9, 845 36, Slovakia*
[c] *FunGlass, Alexander Dubček University of Trenčín, Študentská 2, Trenčín, SK-911 50, Slovakia*

Abstract

Viscosity and structural relaxation were studied by thermomechanical analysis for six Al_2O_3-doped $BaO-P_2O_5$ glasses. The low-temperature viscosity data (10^7 - 10^{11} Pa·s) were described and modeled by the Vogel-Fulcher-Tammann, Avramov-Milchev and Mauro-Yue-Ellison-Gupta-Allan equations. Temperature dependence of the activation energy of viscous flow was determined from the tangent of the extrapolated (in terms of the three viscosity equations) viscosity-temperature data-curves. Values of the activation energy of viscous flow were compared to the activation energies of volume relaxation determined from the exact physico-chemical description of the cyclic thermomechanical measurements performed over the glass transition region. In addition, differential scanning calorimetry was used to determine the activation energies of enthalpy relaxation. Good correspondence between the relaxation and viscosity activation energies was found in the respective temperature ranges. Good agreement was also confirmed for the viscosity and enthalpy fragilities, as well as for the indicator of the thermodynamic fragility.

Keywords: activation energy; viscosity; structural relaxation; TMA; $BaO-P_2O_5-Al_2O_3$ glasses

1. Introduction

Kinetics of the glass transition phenomenon has been explored, described and reviewed for several decades now. [1-10] Despite the massive effort, the present models still have their shortcomings and no general consensus has been reached over the physical interpretation of the phenomenology. For example, nowadays, the probably most famous and most often utilized model for description of structural relaxation kinetics is still the four-parameter phenomenological Tool-Narayanaswamy-Moynihan model (TNM) [11-13] developed in 1946. This model has certain flaws [14] that were still not fully addressed, but the procedural routines for its usage are well developed (see e.g. [15-17] for some recent advancements on this field) and even attempts towards the physico-chemical interpretation of the TNM parameters were made [18-20].

Majority of scientific reports dealing with the glass transition kinetics focus on the activation energy of this process. [21-30] It is indeed the most important parameter, as it determines the position of the glass transition phenomenon with respect to the temperature axis and describes its shift/evolution with experimental conditions (temperature T, heating or cooling rate q^+ / q^-, applied stress, etc.). One of the other proposed meanings of the activation energy of structural relaxation is its similarity with the activation energy of viscous flow in the corresponding temperature region [31, 32] – the idea is based on the concept of the structural relaxation movements being mechanistically (on the atomic level) similar to the structural changes associated with the flow of the matter. Conformity of these two processes has been recently reported for the case of selenium glassy matrix [33]. However, papers dealing with this question are still very rare, despite the fact that the potential confirmation of this correlation for various groups of amorphous materials would result in a significantly increased efficiency of the high-viscosity measurements and it would also greatly contribute to understanding of the nature of the structural relaxation movements.

The present paper will be focused at the comparison of the activation energies obtained for enthalpic and volume structural relaxations and viscous flow for the family of BaO-P_2O_5-Al_2O_3 glasses. The barium phosphate glassy materials have numerous applications, including e.g. fiber amplifiers in the 1.55 telecommunication window [34], Faraday-effect-based optical current sensors [35], production of athermal glassy components [36] and optical filters [37], or radiation shielding materials [38]. Addition of low amount of Al_2O_3 in the phosphate glass matrix then provides increased chemical stability of the glass. [39] Considering the wide range of potential new applications for the barium phosphate glasses with increased chemical resistance, the possibility to predict their workability (dictated by the viscous behavior) and long-term stability (determined by the structural relaxation processes) will be of crucial importance.

2. Experimental

A compositional series of Al_2O_3-doped barium phosphate glasses was prepared by the standard melt-quench approach. The glasses were prepared from analytical grade ammonium dihydrogen phosphate ($NH_4H_2PO_4$) and barium carbonate ($BaCO_3$) (listed in Table 1). [53] Final composition of the Al_2O_3-doped barium phosphate glasses was determined by X-ray fluorescence elemental analysis (XRF), using the S8 Tiger spectrometer (Bruker) – see Table 1. Structure of the prepared glass batches was characterized by using the Renishaw inVia Reflex Raman spectrometer with a Leica DM2500 microscope; a semiconductor ($\lambda = 532$ nm) laser with ~ 28.5 mW power was used as an excitation source. Amorphous character of the prepared glass batches was verified by using the X-ray diffractometer (XRD) Panalytical Empyrean DY1098 (CuKα radiation in the θ-2θ arrangement).

Viscosity and volume relaxation measurements were performed, using the thermomechanical analyzer TMA 402 (Netzsch), on prismatic samples cut (via low-speed

diamond-wheel saw) from the originally prepared glass batches. Approximate sample dimensions were 5x5x20 mm with the masses ranging in-between 16 – 20 g. Both types of measurements were performed based on the axial deformation of the prismatic sample under constant load of 50 mN. The viscosity measurements were performed isothermally, at temperatures covering the viscosity range of approx. 10^7- 10^{11} Pa·s. Volume relaxation measurements were realized based on a non-isothermal cyclical temperature program with alternating cooling and heating steps performed over the T_g region (heating rates q^+ were always the same as was the rate of the preceding cooling q^-, i.e. 5 °C·min^{-1}). The temperature ranges for the TMA cyclic experiments are for all studied glass batches listed in Table 2.

The enthalpy relaxation measurements were realized by using the heat-flow differential scanning calorimeter DSC Q2000 (TA Instruments). The instrument was calibrated using In, and Zn; dry N_2 was used as purge gas at a flow rate of 50 cm^3·min^{-1}. The sample masses were approximately 8 - 10 mg. Cyclic temperature program based on the concept of the constant ratio (CR) cycles [40] was used, where the sample was cyclically cooled and heated through the glass transition region and the heating rates q^+ were always the same as was the rate of the preceding cooling q^-. The temperature ranges for the DSC cyclic experiments are for all studied glass batches listed in Table 2.

3. Results

Amorphous character of the six prepared glassy batches was confirmed by XRD, where none of the diffraction patterns showed distinct diffraction lines, only typical very weak amorphous halos could be recognized (the XRD patterns are included in the Supplementary online material). Structure of the prepared glasses was investigated by means of Raman spectroscopy – see Fig. 1 for the obtained Raman spectra. Assignment of the Raman bands can be done as follows: the spectral region 250 – 560 cm^{-1} includes bands

corresponding to internal vibrations such as deformation vibrations of phosphate chains and PO_3 deformation vibrations of pyrophosphate segments [41], 680 cm^{-1} corresponds to symmetrical stretching vibration of bridging oxygen atoms in Q^2 units [42], 1012 cm^{-1} corresponds to symmetrical stretching vibration of non-bridging oxygen atoms in Q^1 units terminating the metaphosphate chains [42,43], 1161 cm^{-1} corresponds to symmetrical stretching vibration of non-bridging oxygen atoms in Q^2 units [41,43,44], 1250 - 1300 cm^{-1} corresponds to asymmetric stretching vibration of the two non-bridging oxygen atoms bonded to phosphorus atom [45,46]. Compositional evolution of the above-mentioned bands intensities is in a good correspondence with the elemental analysis provided by XRF (see Table 1).

Viscosity behavior was studied based on the measurements of the axial deformation of the prismatic sample under constant load:

$$\eta = \frac{Fl}{3S(dl/dt)} \quad (1)$$

where F is the applied loading force, l stands for the height of sample, S stands for the sample cross-section (in the direction of applied force), and dl/dt is the deformation rate. The temperature dependences of viscosities determined for the six $BaO\text{-}P_2O_5\text{-}Al_2O_3$ glasses at arbitrarily selected temperatures are shown in Fig. 2. Positions of the particular η-T dependences very well correspond to the compositional changes within the two sub-series of prepared glasses (as presented in Table 1). Glasses Nos. 4 – 6 have rather high (and similar) Al_2O_3 content, which results in large increase of viscosity (and the corresponding shift of the measured η-T dependences to higher temperatures) – the tetrahedral Al ions cross-link with the neighboring phosphor chains by the formation of $AlPO_4$ species that strengthen the glass network [47]. Also the addition of the modifier oxide BaO leads to a significant increase of the glass matrix interconnectivity, as it forms a polyhedron, being surrounded by two Q^2 and several Q^3 PO_4 tetrahedrons [47]. Considering the second sub-series composed of the glasses

Nos. 1 – 3 (with low, varying amount of Al_2O_3 being added), it is apparent that the increase of the isoviscous temperature associated with the addition of Al_2O_3 is more than tenfold compared to the contribution of BaO (compared mole-to-mole based on the XRF-determined compositions listed in Table 1).

Apart from the determination of viscosity, the TMA technique was also used to perform the non-isothermal cyclic volume relaxation measurements. Since the upper temperature limit was set at values above the softening point, simultaneous modeling of the structural relaxation, thermal expansion/contraction and viscous flow had to be done. Accounting for the contributions of all three processes, the sample strain ε (relative sample length change) can be defined as:

$$\varepsilon = \frac{l_2 - l_1}{l_1} \approx \int_{T_1}^{T_2} \alpha_g dT + \int_{T_{f,1}}^{T_{f,2}} \Delta\alpha dT_f - \left(1 + \int_{T_1}^{T_2} \alpha_g dT + \int_{T_{f,1}}^{T_{f,2}} \Delta\alpha dT_f\right) \int_{t_1}^{t_2} \frac{\sigma}{3\eta(T, T_f)} dt \quad (2)$$

where α_g and α_m are the thermal expansion coefficients of glass and undercooled liquid/melt, $\Delta\alpha$ is defined as $\Delta\alpha = \alpha_m - \alpha_g$, T is temperature, t is time, T_f is the Tool's [11] fictive temperature defined as the temperature at which the undercooled liquid would have the same structure as is that of the relaxing glass, σ is the axial stress and η is viscosity. Evolution of the fictive temperature with time can be expressed as:

$$T_f(T) = T(t) - \int_0^t dt' \left(\frac{dT}{dt}\right) M[\xi(t) - \xi(t')] \quad (3)$$

$$M(\xi) = \exp(-\xi^\beta) \quad (4)$$

$$\xi(t) = \int_0^t \frac{dt'}{\tau(t')} = \int_0^t \frac{K}{\eta(t')} dt' \quad (5)$$

where M is the Kohlrausch-Williams-Watts [48,49] relaxation function, ξ is the dimensionless relaxation time, β is the non-exponentiality relaxation parameter and K is the shear modulus.

In the present work, the relaxation model used to quantify ξ in dependence on T and T_f was the Tool-Narayanaswamy-Mazurin (TNMa) [50] expressed by Eq. 6:

$$\log \eta(T,T_f) = \left(A + \frac{B}{T - T_0} \right) \frac{T_f}{T} + \log \eta_0 \left(1 - \frac{T_f}{T} \right) \tag{6}$$

where A, B and T_0 are the coefficients of the Andrade viscosity equation [51] and η_0 is the limit dynamic viscosity.

The experimental TMA (volume) relaxation data described by the set of Eqs. 2 – 7 are shown in Fig. 3. The non-linear regression analysis was performed by the self-made non-commercial software written in Fortran [52, 53] – the resulting values of the relaxation parameters are listed in Table 3. Very good agreement between the experimental data and theoretical TNMa description was achieved, as is demonstrated by the Fisher's F-statistics and standard deviation of approximation s_{apr} listed in Table 3. Since the present paper is primarily focused on the values of activation energies, we have correlated the E_{rel} from Table 3 with the information on the glass compositions from Table 1. A very reasonable correlation coefficient (defined via Eq. 7) of r = 0.85 was obtained for the correlation between E_{rel} and the BaO content (the correlation coefficient increased to r = 0.93 when omitting the data for the glass No. 6). Hence, contrary to the isoviscous temperatures, the activation energy determined by non-linear optimization from the non-isothermal cyclic TMA measurements appears to be driven mostly by the BaO-P_2O_5 interaction, with the Al_2O_3 doping playing only minor role.

$$r = \frac{\sum (x - \bar{x})(y - \bar{y})}{\sqrt{\sum (x - \bar{x})^2 \sum (y - \bar{y})^2}} \tag{7}$$

The activation energy of the structural relaxation processes in the six prepared BaO-P_2O_5-Al_2O_3 glasses was also determined from the DSC non-isothermal cyclic experiments based on the CR cycles concept [40]. Typical example of the DSC CR cycles is (for the glass

No. 1) shown in Fig. 4A. Compared to the description of the TMA relaxation cycles (Eqs. 2 – 7), explicit formulation of the heat flow temperature dependence during the DSC experiment is much more complicated due to the three-dimensional problem of heat transfer and heat losses, coupled with the difficult-to-define thermal gradients within the sample and the DSC cell. For this reason, usually only the pure relaxation signal (heat capacity normalized according Eq. 8) is being modeled by the TNMo phenomenology (combination of Eqs. 3, 4, 5 and 9) as described e.g. in [15].

$$C_p^{red} = \frac{dT_f}{dT} = \frac{C_p(T) - C_{pg}(T)}{C_{pl}(T) - C_{pg}(T)} \tag{8}$$

$$\log \tau(T, T_f) = A' + x\frac{\Delta h^*}{RT} + (1-x)\frac{\Delta h^*}{RT_f} \tag{9}$$

where C_p^{red} is the normalized heat capacity, C_p is the experimentally determined heat capacity, and C_{pl} and C_{pg} are the extrapolated heat capacities in the undercooled liquid and glassy states, respectively. In Eq. 9 the quantity A' is the TNMo pre-exponential factor, x is the non-linearity parameter and Δh^* is the apparent activation energy of enthalpic relaxation. Nevertheless, if one is interested only in the apparent activation energy Δh^*, the recently introduced linearization method [17] derived on the basis of the TNMo phenomenology can be utilized. Since the method utilizes only the values of the temperatures corresponding to the maxima of the DSC relaxation peaks occurring during the CR cycles, it is very accurate and robust at the same time – as was shown e.g. in [40]. The Δh^* determination is based on Eqs. 10 and 11:

$$-\frac{\Delta h^*}{R} = \left[\frac{d \ln|q^+|}{d(1/T_P)}\right]_{q^-/q^+ = const} \tag{10}$$

$$\Delta h^*_{e.v.} = 4.218 \cdot 10^{-5} z^2 + 4.841 \cdot 10^{-2} z + \left[9.885 \cdot 10^1 / (z - 1.276)\right] \tag{11}$$

where T_p is the temperature corresponding to the maximum of the relaxation peak (overshoot), q^+ is the heating rate, z stands for the true value of $\Delta h^*/R$, and $\Delta h^*_{e.v.}$ represents the percent error value defined [17] as:

$$\Delta h^*_{e.v.} = \frac{1}{63} \times \sum_{i,j}^{x,\beta} \frac{\left(\Delta h^*_{\exp.,ij} - \Delta h^*_{teor.}\right)}{\Delta h^*_{teor.}} \times 100\% \qquad (12)$$

where Δh^*_{exp} and Δh^*_{teor} are the experimentally determined (via Eq. 10) and true (z from Eq. 11) values of the apparent activation energy of enthalpy relaxation, respectively.

The $\ln q^+$ vs. $1/T_p$ dependences obtained from the DSC CR cycles for the studied BaO-P_2O_5-Al_2O_3 glasses are shown in Fig. 4B. Reasonable linearity of the dependences indicates that no data-distortive thermal gradients occurred within the samples even for the highest applied q^+. [40] Similarly to the η-T dependences depicted in Fig. 2, also the $\ln q^+$-$1/T_p$ dependences shown in Fig. 4B exhibit the expected compositional shifts along the temperature axis, where the increase of T_g associated with the addition of Al_2O_3 is largely higher compared to that caused by increasing BaO content. Note however, that the mutual positions of the particular dependences is slightly different for η-T and for $\ln q^+$-$1/T_p$. This indicates that the influence on glass network connectivity evolves with temperature differently for the Al_2O_3 and BaO components (viscosity was measured at higher temperatures compared to the enthalpic relaxation).

5. Discussion

In order to correlate the activation energies of structural relaxation and viscous flow, the η-T dependences depicted in Fig. 2 had to be extrapolated to lower temperatures. Compared to the isothermally obtained equilibrium viscosities (measured in the 10^7 - 10^{11} Pa·s range), the enthalpy relaxation was technically determined only in close vicinity of T_g (i.e. at around $10^{12} - 10^{12.5}$ Pa·s) and the volume relaxation measured by TMA was measured (and described – see Fig. 3) from the sample softening down to well below T_g

(between approx. 10^8 Pa·s to the > 10^{16} Pa·s viscosity range). To achieve the extrapolations, the viscosity data from Fig. 2 were independently described by three equations with distinct predictive behavior:

$$\log \eta = \log \eta_0 + \frac{B}{T - T_0} \tag{13}$$

$$\log \eta = \log \eta_0 + \frac{B'}{T^{C'}} \tag{14}$$

$$\log \eta = \log \eta_0 + \frac{B''}{T} \cdot \exp\left(\frac{C''}{T}\right) \tag{15}$$

where η_0, B, B', B'', T_0, C' and C'' are optimizable parameters. The equations are known as the Vogel-Fulcher-Tammann [54-56] (VFT; Eq. 13), Avramov-Milchev [57] (AM; Eq. 14) and Mauro-Yue-Ellison-Gupta-Allan [58] (MYEGA; Eq. 15) models. The description of the viscosity data obtained for the BaO-P_2O_5-Al_2O_3 glasses is shown in Fig. 5. Note that in theory two alternative fits can be performed with respect to the parameter η_0. Either the parameter η_0 can be fixed during the nonlinear optimization at the value $\eta_0 = 4 \cdot 10^{-5}$ Pa.s in accordance with the Eyring theory [59] (the results are shown in Fig. 5 and listed in Table 4) or it can be set free for optimization (the results are included in the Supplementary online material). As is apparent from Fig. 5, all three models (Eqs. 13 – 15) describe the data reasonably well but lead to slightly different estimates when extrapolated outside of the experimentally measured range. The fits are of roughly comparable precision in case of all viscosity equations – see the respective sums of squared residue SSR in Fig. 5. For the present data the flexibility of the viscosity equations (and the corresponding precision of the least squares fits) decreases in the following order: MYEGA → VFT → AM. Compared with the unrestricted fits (see the Supplementary online material), the Eyring restriction [59] obviously results in higher SSR due to the forced higher curvature of the dependences. However, often only a marginal

increase of SSR was observed and the difference was almost always within one order of magnitude.

With the logη-T^{-1} data being described, the activation energy of viscous flow can be calculated from the tangent of the dependence as:

$$E_\eta = 2.303 \cdot R \cdot \frac{d(\log \eta)}{d(1/T)} \tag{16}$$

This calculation was performed for all three tested viscosity equations (VFT, AM and MYEGA) based on the extrapolations simulated for the parameters listed in Table 4. Note that the true derivation of the viscosity data shown in Fig. 5 would provide very few points exhibiting high scatter. Instead, the logη-T^{-1} data were simulated with high datapoint density in a large/extrapolated temperature range based on the corresponding sets of parameters from Table 4 and, consequently, these dependences were derived according Eq. 16. In addition, also the parameters obtained from the unrestricted fits (see Supplementary online material) were processes in a similar way and the corresponding findings are again listed in the Supplementary online material. The obtained E_η-T dependences are for the studied BaO-P_2O_5-Al_2O_3 glasses depicted in Fig. 6 together with the values of apparent activation energies of structural relaxation obtained from the TMA and DSC cyclic experiments. Note that for Δh^* the points correspond to the temperature values from Fig. 4B, whereas in case of E_{rel} the line indicates the temperature interval from T_g onset to the sample softening temperature (where the interaction between the structural relaxation and viscosity is within the experimentally observed time window). As is apparent, each viscosity equation provides a different characteristic curvature of the predicted temperature dependence of E_η – for the present data the steepness of the E_η decrease with increasing T increases as follows: VFT → MYEGA → AM. Note that in case of the fits of the viscosity data unrestricted by the Eyring condition [59] the general course of the E_η-T dependences (positive/negative slope, steepness of the decrease/increase) and the trends in the corresponding predictions largely vary for all

equations utilized in the present work. It is therefore highly recommended to use the Eyring restriction [59] in order to obtain reliable and consistent interpretations and predictions of the η-T dependences.

Regarding the correlation between the activation energies of viscous flow and structural relaxation, good correlation was obtained between E_η (predicted by practically all tested viscosity equations) and E_{rel} obtained from the TMA measurements described by TNMa model. One of course needs to bear in mind that the red horizontal lines in Fig. 6 account for the whole temperature range measured by TMA and that the true glass transition region (the structural relaxation of which is actually described by the TNMa model) is located at the right-hand end of those lines. Whereas activation energies of different processes (viscous flow vs. structural relaxation) are being correlated, the measurements are performed via the same instrument, utilizing the same physical quantity and similar temperature range. Different situation arises in case of the enthalpy relaxation activation energy Δh^*, where for glasses Nos. 1 – 4 the Δh^* values are higher (by up to 20 %) compared to E_{rel}. Note that in theory there is no reason for the enthalpy relaxation to exhibit similar activation energy as the volume relaxation because both quantities (enthalpy and volume) may behave/manifest differently in reaction to the same structural movements. Although Δh^* is relatively close to the E_η predicted by VFT (not so much by MYEGA and AM) for the given temperature range, the reverse relationship, which would enable the desired prediction of E_η (quantity tedious to obtain) from the Δh^* data (which are quick and easy to obtain), cannot be confirmed based on the present data. Regarding the glasses Nos. 5 and 6, their Δh^* correlates very well with E_{rel}. At the moment, we have no explanation for the marked difference between the two types of Δh^* behavior – there is no clear relationship between the Δh^* disparity and T_g, E_η/T_g, T_{soft}/T_g (with T_{soft} being the softening point) or structural ordering/interconnectivity (as inferred from the compositions listed in Table 1).

In addition to the activation energies, also the kinetic fragilities (in accordance with the Angell classification [8]) defined via the following expressions were calculated:

$$m_{visc.} = \left.\frac{d\log\eta}{d(T_g/T)}\right|_{T=T_g} \cong \frac{E_\eta/R}{T_g\ln(10)} \tag{17}$$

$$m_{h^*} = \left.\frac{d\log\tau}{d(T_g/T)}\right|_{T=T_g} \cong \frac{\Delta h^*/R}{T_g\ln(10)} \tag{18}$$

The fragilities calculated from the E_η-T dependences are denoted m_{VFT}, m_{AM} and m_{MYEGA} – see Table 5. Moreover, several other parameters [62] associated with the kinetic fragilities are also listed in Table 5: D^* calculated from the VFT description as B/T_0, and the ratio of B''/C'' parameters from the MYEGA equation. Finally, Δc_p obtained from the DSC measurements as the difference between the heat capacities of the glassy and undercooled liquid states is listed in Table 5 as a representation of the thermodynamic fragility concept [8] (Δc_p is proportionate to the configurational entropy frozen-in at T_g).

Starting with $m_{visc.}$, the absolute values provided by the different viscosity equations show quite large variations due to the different extrapolated E_η-T courses resulting from the respective mathematic expressions (Eqs. 13 – 15); however, the compositional trends of $m_{visc.}$ are similar for all three viscosity equations. This demonstrates the importance of a consolidated approach to evaluation, comparison and interpretation of the (fragility) data obtained via extrapolation of the measured values. Interestingly, the comparison of the viscosity and enthalpy kinetic fragilities shows a very good agreement between m_{AM} and m_{h^*} for the glasses Nos. 1 – 4, which may suggest that it is actually the higher Δh^* values which are consistent with the viscosity data (see the discussion to Fig. 6 in the previous paragraph). Also the D^* parameter shows very good correlation with the $m_{visc.}$ data (note that the correlation is inverse [62], i.e. high D^* indicates strong behavior). Similarly good correlation is found also for the B''/ C'' ratio, which (similarly as in [62]) shows almost linear increase with D^* - the correlation coefficient for the linear increase is $r = 0.987$. Regarding the

thermodynamic fragility, Δc_p shows a reasonable correlation with the kinetic fragility parameters listed in Table 5 – the correlation coefficient *r* varies between 0.81 and 0.90 depending on the kinetic fragility parameter. Compositionally, the interpretation of the fragility parameters is rather straightforward – decrease of the glass structure rigidity is associated with increase of materials fragility. This is in a good agreement with the present data, where the glasses with high BaO content (this modifier oxide increases the matrix interconnectivity, introducing variability into the system structure [47]) exhibit higher fragility indices. Note that the Al_2O_3 content appears o have practically no influence on the resulting fragility value.

6. Conclusions

Thermomechanical analysis and differential scanning calorimetry were used to study the relationship between the activation energies of viscous flow and structural relaxation for the Al_2O_3-doped BaO-P_2O_5 glasses. Temperature dependences of viscosity were measured in the 10^7 - 10^{11} Pa·s range and described by the VFT, AM and MYEGA equations. Cyclic volume relaxation experiments performed using TMA were modeled in terms of the TNMa model in a wide temperature range starting well below T_g and ending slightly above the glass softening point. Activation energy of enthalpy relaxation was determined by the peak-shift method from the constant-ratio cyclic DSC measurements. Very good correspondence was found between the activation energy of volume relaxation E_{rel} (TMA) and the activation energy of viscous flow determined by all viscosity equations.

The enthalpy relaxation activation energies Δh^* exhibited reasonable correspondence with the activation energies of viscous flow determined via the VFT equation (the extrapolated data provided by the other two equations showed worse correspondence with Δh^*). Significant difference between Δh^* and E_{rel} was found in case of four BaO-P_2O_5-Al_2O_3

glasses; these quantities were similar only in case of two glasses out of the six tested. However, good agreement was observed between the viscosity and enthalpy kinetic fragilities of the four glasses with significantly different Δh^* and E_{rel}, which indicates that the difference in relaxation activation energies is caused by the different temperature range in which they were evaluated (it also indicates that the two materials with similar Δh^* and E_{rel} are in fact anomalous). It should be noted that structural relaxation can exhibit different kinetics when experienced via different quantities (volume vs. enthalpy) [60, 61], and there is in fact no reason why the two physical properties should react in the exactly same way on the structural changes in glassy matrix.

Acknowledgments

This work was supported by The Slovak Grant Agency for Science under grant No. VEGA 2/0088/16, and VEGA 1/0064/18, and the project Centre for Functional and Surface Functionalized Glass (CEGLASS), ITMS code is 313011R453, operational program Research and innovation, co-funded from European Regional Development Fund.

References

[1] W. Gotze, L. Sorjen. Relaxation processes in supercooled liquids. Rep. Prog. Phys. 55 (1992) 241-376.
[2] M.D. Ediger. Spatially heterogeneous dynamics in supercooled liquids. Annu. Rev. Phys. Chem. 51 (2000) 99-128.
[3] R. Brand, P. Lunkenheimer, A. Loidl. Relaxaton dynamics in plastic crystals. J. Chem. Phys. 116 (2002) 10386-10401.
[4] J.-L. Barrat, J. Baschnagel, A. Lyulin. Molecular dynamics simulations of glassy polymers. Soft Matter 6 (2010) 3430-3446.
[5] M. Alcoutlabi, G.B. McKenna. Effects of confinement on material behaviour at the nanometre size scale. J. Phys.-Condens. Mat. 17 (2005) 461-524.
[6] C.A. Angell, K.L. Ngai, G.B. McKenna, P.F. McMillan, S.W. Martin. Relaxation in glassforming liquids and amorphous solids. J. Appl. Phys. 88 (2000) 3113-3157.
[7] L. Berthier, G. Biroli. Theoretical perspective on the glass transition and amorphous materials. Rev. Mod. Phys. 83 (2011) 587-645.
[8] C.A. Angell. Relaxation in liquids, polymers and plastic crystals – strong fragile patterns and problems. J. Non-Cryst. Sol. 131 (1991) 13-31.
[9] D. Cangialosi, V.M. Boucher, A. Alegria, J. Colmenero. Physical aging in polymers and polymer nanocomposites: recent results and open questions. Soft Matter 9 (2013) 8619-8630.

[10] Q. Zheng, Y. Zhang, M. Montazerian, O. Gulbiten, J.C. Mauro, E.D. Zanotto, Y. Yue. Understanding glass through differential scanning calorimetry. Chem. Rev. 119 (2019) 7848-7939.
[11] A. Q. Tool. Relation between inelastic deformability and thermal expansion of glass in its annealing range. J. Am. Ceram. Soc. 29 (1946) 240.
[12] O. S. Naraynaswamy. A model of structural relaxation in glass. J. Am. Ceram. Soc. 54 (1971) 491.
[13] C. T. Moynihan, A. J. Easteal, M. A. DeBolt, J. Tucker. Dependence of the fictive temperature of glass on cooling rate. J. Am. Ceram. Soc. 59 (1976) 12.
[14] A. J. Kovacs. Glass transition in amorphous polymers: a phenomenological study. Fortschr. Hochpolym. Forsch., 3 (1963) 394.
[15] R. Svoboda, J. Málek. Description of macroscopic relaxation dynamics in glasses. J. Non-Cryst. Solids 378 (2013) 186-195.
[16] R. Svoboda. How to determine activation energy of glass transition. J. Therm. Anal. Calorim. 118 (2014) 1721-1732
[17] R. Svoboda. Novel equation to determine activation energy of enthalpy relaxation. J. Therm. Anal. Calorim. 121 (2015) 895-899.
[18] R. Svoboda. Relaxation processes in selenide glasses: Effect of characteristic structural entities. Acta Materialia 61 (2013) 4534-4541
[19] J.M. Hutchinson. Physical aging of polymers. Prog. Polym. Sci. 20 (1995) 703-760.
[20] J.M. Hutchinson. Interpretation of glass transition phenomena in the light of the strength-fragility concept. Polym. Inter. 47 (1998) 56-64.
[21] B.J. Fernandes, K. Ramesh, N.K. Udayashankar. Crystallization kinetics of $Si_{20}Te_{80-x}Bi_x$ ($0 < x < 3$) chalcogenide glasses. Mat. Sci. Eng. B 246 (2019) 34-41.
[22] S.K. Pal, N. Chandel, N. Mehta. Synthesis and thermal characterization of novel phase change materials (PCMs) of the Se-Te-Sn-Ge (STSG) multi-component systém: calorimetric studies of glass/crystal phase transition. Dalton Trans. 48 (2019) 4719-4729.
[23] D.E. Lee, H.-J. Cho, B.-S. Kong, H.O. Choi. Investigation on curing characterization of epoxy molding compounds with different latent catalysts by thermal, electrical and mechanical analysis. Thermochim. Acta 674 (2019) 68-75.
[24] K.H. Sadok, M. Haouari, O. Gallot-Lavalée, H.B. Ouada. Effect of Na_2SO_4 substituion for Na_2O on the structural and electrical properties of a sodium borophosphate glass. J. Alloys. Compd. 778 (2019) 878-888.
[25] A. Afzal, M.S. Thayyil, P.A. Sivaramakrishnan, M.K. Sulaiman, K.P.S. Hussan, C.Y. Panicker, K.L. Ngai. Dielectric spectroscopic studies in supercooled liquid and glassy states of Acemetacin, Brucine and Colchicine. J. Non-Cryst. Sol. 508 (2019) 33-45.
[26] M.M. Abutalib. Effect of zinc oxide nanorids on the structural, thermal, dielectric and electrical properties of polyvinyl alcoholcorboxymethyle cellulose composites. Phys. B. 557 (2019) 108-116.
[27] M.I. Abd-Elrahman, M. Sayed, A.A. El-Fadl, A.A. Abu-Sehly, M.M. Hafiz. The activation energies at glass transition temperatures and dynamic fragility of $(Se_{90}Te_{10})_{100-x}In_x$ glassy alloys. Thermochim. Acta 672 (2019) 86-92.
[28] E.B. Yekta, M. Adineh, H. Nasiri, H. Shalchian. A new soft magnetic $Fe_{75}Ta_5C_{20}$ amorphous alloy: Modelling and kinetics approach. J. Alloys Compd. 773 (2019) 537-547.
[29] S. Saini, A.P. Srivastava, S. Neogy. The effect of Ag addition on the crystallization kinetics and glass forming ability of Zr-(CuAg)-Al bulk metallic glass. J. Alloys Compd. 772 (2019) 961-967.

[30] G. Abbady, A.M. Abd-Elnaiem. Thermal stability and crystallization kinetics of $Ge_{13}In_8Se_{79}$ chalcogenide glass. Phase Trans. 92 (2019) 667-682.
[31] I. M. Hodge. Adam-Gibbs formulation of nonlinear enthalpy relaxation. J. Non-Cryst. Sol. 131–133 (1991) 435-441.
[32] M. Chromčiková and M. Liška. Simple relaxation model of the reversible part of the StepScan DSC record of glass transition. J. Therm. Anal. Calorim. 84 (2006) 703-708.
[33] J. Málek, R. Svoboda. Kinetic processes in amorphous materials revealed by thermal analysis: Application to glassy selenium. Molecules 24 (2019) 2725.
[34] S. Jiang, T. Luo, B.-C. Hwang, F. Smekatala, K. Seneschal, J. Lucas, N. Peyghambarian. Er^{3+}-doped phosphate glasses for fiber amplifiers with high gain per unit length. J. Non-Cryst. Solids. 263&264 (2000) 364-368.
[36] H. In, H. Takebe, K. Morinaga. Low photo-elastic characteristics of $BaO-P_2O_5$ glasses. J. Ceram. Soc. Japan. 111 (2003) 426-429.
[37] E.T.Y. Lee, E.R.M. Taylor. Optical and thermal properties of binary calcium phosphate and barium phosphate glasses. Opt. Mater. 28 (2006) 200-206.
[38] E. Metwalli, M. Karabulut, D.L. Sidebottom, M.M. Morsi, R.K. Brow. Properties and structure of copper ultraphosphate glasses. J. Non-Cryst. Solids 344 (2004) 128-134.
[39] B.O. El-Bashir, M.I. Sayyed, M.H.M. Zaid, K.A. Matori. Comprehensive study on physical, elastic and shielding properties of ternary $BaO-Bi_2O_3-P_2O_5$ glasses as a potent radiation shielding material. J. Non-Cryst. Sol. 468 (2017) 92-99.
[40] R. Svoboda. Utilization of "q^+/q^- = const." DSC cycles for enthalpy relaxation studies. Eur. Polym. J. 59 (2014) 180-188
[41] C. Ivascu, A. Timar Gabor, O. Cozar, L. Daraban, I. Ardelean, FT-IR, Raman and thermoluminescence investigation of P2O5–BaO–Li2O glass system, J. Mol. Struct. 993 (2011) 249–253
[42] L.L. Velli, C.P.E. Varsamis, E.I. Kamitsos, D. Möncke, D. Ehrt, Structural investigation of metaphosphate glasses, Phys. Chem. Glasses 46 (2005) 178–181.
[43] I. Konidakis, C.-P.E. Varsamis, E.I. Kamitsos, D. Möncke, D. Ehrt, Structure and properties of mixed strontium–manganese metaphosphate glasses, J. Phys. Chem. C 114 (2010) 9125–9138
[44] C. Ivascu, I.B. Cozar, L. Daraban, G. Damian, Spectroscopic investigation of P2O5–CdO–Li2O glass system, J. Non-Cryst. Solids 359 (2013) 60–64.
[45] T. Harada, H. In, H. Takebe, K. Morinaga, Effect of B2O3 addition on the thermal stability of barium phosphate glasses for optical fiber devices, J. Am. Ceram. Soc. 87 (2004) 408–411
[46] A. Chahine, M. Et-tabirou, M. Elbenaissi, M. Haddad, J.L. Pascal, Effect of CuO on the structure and properties of (50 − x/2)Na2O–xCuO–(50 − x/2)P2O5 glasses, Mater. Chem. Phys. 84 (2004) 341–347
[47] S.V.G.V.A. Prasad, M.S. Reddy, N. Veeraiah. Nickel ion – A structural probe in $BaO-Al_2O_3-P_2O_5$ glass systém by means of dielectric, spectroscopic and magnetic studies. J. Phys. Chem. Sol. 67 (2006) 2478-2488.
[48] R. Kohlrausch. Theorie des elektrischen Rückstandes in der Leidner Flasche. Ann. Phys. Chem. 91 (1854) 179–213.
[49] G. Williams, D.C. Watts. Non-Symmetrical Dielectric Relaxation Behavior Arising from a Simple Empirical Decay Function. Trans. Faraday Soc. 66 (1970) 80-85.
[50] O.V. Mazurin, J.K. Starcev, R.J. Chodakovskaja. Relaxacionnaja teorija otzhiga stekla i raschet na jej osnove rezhimov otzhiga. Moskva: Moskovskij chimikotechnologicheskij institut; 1986.
[51] E.N. Andrade. The viscosity of liquids. Endeavour 12 (1954) 117-127.

[52] M. Liška, I. Štubňa, J. Antalík, P. Perichta. Structural relaxation with viscous flow followed by thermodilatometry. Ceramics-Silikáty 40 (1996) 15-19.
[53] M. Chromčíková, R. Dagupati, R. Svoboda, B. Hruška, M. Liška, F. Munoz. Structure and volume relaxation of selected $BaO-P_2O_5$ glasses. CEEC-TAC5 Book of abstracts (2019) Rome, PS3.076.
[54] H. Vogel. Das Temperaturabhaengigkeitsgesetz der Viskositaet von Fluessigkeiten. Physik Z. 22 (1921) 645.
[55] G.A. Fulcher. Analysis of recent measurements of the viscosity of glasses. J. Am. Ceram. Soc. 8 (1925) 339 – 355.
[56] G. Tammann, W. Hesse. Die Abhangigkeit der Viskositat von der Temperatur bei unterkuhlten Flussigkeiten. Z. Anorg. Allgem. Chem. 156 (1926) 245-257.
[57] I. Avramov, A. Milchev. Effect of disorder on diffusion and viscosity in condensed systems. J. Non-Cryst. Solids 104 (1988) 253.
[58] J. C. Mauro, Y. Yue, A. J. Ellison, P. K. Gupta, D. C. Allan. Viscosity of glass-forming liquids. PNAS 106 (2009) 19780-19784 (2009)
[59] H. Eyring. Viscosity, plasticity, and diffusion as examples of absolute reaction rate. J. Chem. Phys. 4 (1936) 283.
[60] J. Málek, R. Svoboda, P. Pustková, P. Čičmanec. Volume and enthalpy relaxation of a-Se in the glass transition region. J. Non-Cryst. Solids 355 (2009) 264-272
[61] R. Svoboda, P. Pustková, J. Málek. Structural relaxation of polyvinyl acetate (PVAc). Polymer 49 (2008) 3176-3185
[62] S. Hechler, I. Galliano, M. Stolpe, F.-T. Lentes, R. Busch. Analysis of thermophysical properties of lead silicates in comparison to bulk metallic glasses. J. Non-Cryst. Sol. 485 (2018) 66-73.

Figure captions

Fig. 1: Raman spectra for the studied $BaO-P_2O_5-Al_2O_3$ glasses.

Fig. 2: Viscosity data obtained by the TMA parallel-plate method for the studied $BaO-P_2O_5-Al_2O_3$ glasses. Note that several measurements are reproduced – the error bars are approximately 1.5 fold larger compared to the points magnitude.

Fig. 3: TMA volume relaxation cyclic experiments described by the Tool-Narayanaswamy-Mazurin model.

Fig. 4: A) Example of the constant ratio (CR) cyclic DSC experiments performed for glass No. 1.
B) The $\ln q^+$ vs. $1/T_p$ dependences obtained from the DSC CR cycles for the studied $BaO-P_2O_5-Al_2O_3$ glasses. The error bars are less than the points magnitude.

Fig. 5: Viscosity data obtained for the studied $BaO-P_2O_5-Al_2O_3$ glasses (see Fig. 2) fitted by the VFT, AM and MYEGA models. The error bars for the viscosity data are less than the points magnitude.

Fig. 6: Activation energies of viscous flow E_η calculated from the extrapolated VFT, AM and MYEGA fits (see Fig. 5) compared to the activation energy of volume relaxation E_{rel} and activation energy of enthalpy relaxation Δh^* for the studied $BaO-P_2O_5-Al_2O_3$ glasses. Errors for E_{rel} are listed in Table 3, errors for Δh^* are approximately double the points size.

Tables

Table 1: The composition (wt % and mol %) and abbreviation of studied glasses. The compositional determination errors are in the order of the last listed digit.

Glass No.	P_2O_5 /BaO mol %	P_2O_5 wt %	P_2O_5 mol %	BaO wt %	BaO mol %	Al_2O_3 wt %	Al_2O_3 mol %
1	0.74	40.65	42.53	59.35	57.47	0.00	0.00
2	1.00	47.64	49.40	51.67	49.60	0.70	1.01
3	1.30	53.99	55.59	44.85	42.75	1.16	1.66
4	0.65	36.83	38.33	61.54	59.30	1.63	2.36
5	1.00	47.32	48.85	50.98	48.71	1.70	2.44
6	0.90	44.74	46.27	53.56	51.28	1.70	2.45

Table 2: Temperature ranges for the TMA and DSC cyclic experiments used for the studied $BaO\text{-}P_2O_5\text{-}Al_2O_3$ glasses.

Glass No.	TMA (°C)	DSC (°C)
1	292 – 498	320 – 525
2	282 – 450	270 – 475
3	274 – 460	250 – 500
4	294 – 553	420 – 550
5	294 – 510	300 – 525
6	292 – 481	300 - 525

Table 3: The values of optimized parameters of TNMa relaxation model obtained by non-linear regression analysis of the thermomechanical experimental data. standard deviations of approximation. s_{apr}. of $\Delta l/l_0$ experimental values. and Fisher's F-statistics.

TNMa Parameters	**No.1**	**No.2**	**No.3**	**No.4**	**No.5**	**No.6**
log{K/dPa}	8.70 ± 0.03	8.90 ± 0.02	9.10 ± 0.02	9.27 ± 0.02	8.99 ± 0.02	8.80 ± 0.19
b	0.520 ± 0.007	0.530 ± 0.009	0.570 ± 0.008	0.530 ± 0.006	0.426 ± 0.006	0.490 ± 0.007
B[K]	43 413 ± 5	26 436 ± 3	23 348 ± 2	47 065 ± 2	37 827 ± 2	27 343 ± 3
E[kJ.mol^{-1}]	812 ± 0.1	495 ± 0.1	437 ± 0.1	881 ± 0.1	708 ± 0.1	512 ± 0.1
log{η_0/dPa.s}	-12.13 ± 0.61	-14.52± 0.65	-13.68± 0.50	-13.68 ± 0.54	-29.40 ± 0.94	-13.67 ± 0.56
$10^4 s_{apr}$	0.40781	0.49268	0.45412	0.30735	0.33098	0.45209
F	9 073	7 406	9 543	27 430	17 228	8 632

Table 4: Parameters of the VFT, AM and MYEGA equations obtained for the fits of the BaO-P_2O_5-Al_2O_3 viscosity data. Parameter $\log\eta_0$ in the equations fixed at $\eta_0 = 4\cdot10^{-5}$ Pa.s according [59]. The errors are in the order of the second listed digit; the increased precision is shown in order to list the exact values used for the predictions.

Glass No.	VFT model			AM model			MYEGA model		
	$\log\eta_0$	B	T_0	$\log\eta_0$	logB’	C’	$\log\eta_0$	B’’	C’’
1	-4.398	5498	584.3	-4.398	13.013	3.998	-4.398	880	2507
2	-4.398	7426	470.3	-4.398	9.332	2.750	-4.398	3466	1311
3	-4.398	8773	435.3	-4.398	8.327	2.393	-4.398	5093	1059
4	-4.398	5677	630.9	-4.398	13.279	4.050	-4.398	839	2773
5	-4.398	6366	568.2	-4.398	12.342	3.756	-4.398	1559	2116
6	-4.398	8167	477.1	-4.398	9.175	2.677	-4.398	3793	1334

Table 5: Kinetic fragilities calculated from the VFT, AM and MYEGA predictions; kinetic fragility calculated from the DSC data; D^*_{VFT} calculated as B/T_0; B’’/C’’ ratio from the MYEGA equation; Δc_p obtained from the DSC measurements as the difference between the heat capacities of the glassy and undercooled liquid states. With the exception of Δc_p, the errors of the listed values are in the order of the second listed digit.

Glass No.	m_{VFT}	m_{AM}	m_{MYEGA}	m_{h*}	D^*_{VFT}	$(B''/C'')_{MYEGA}$	Δc_p
	-	-	-	-	-	-	$J\cdot g^{-1}\cdot K^{-1}$
1	82.0	65.5	72.7	67.3	9.41	880	0.771±0.017
2	55.5	45.1	48.8	43.3	15.79	3466	0.716±0.011
3	47.1	39.2	42.5	44.0	20.15	5093	0.729±0.018
4	85.0	66.3	74.6	63.6	9.00	839	0.780±0.005
5	71.5	61.5	63.5	44.8	11.20	1559	0.748±0.019
6	52.5	43.9	48.0	36.9	17.12	3793	0.744±0.013

Figure 1

Click here to download high resolution image

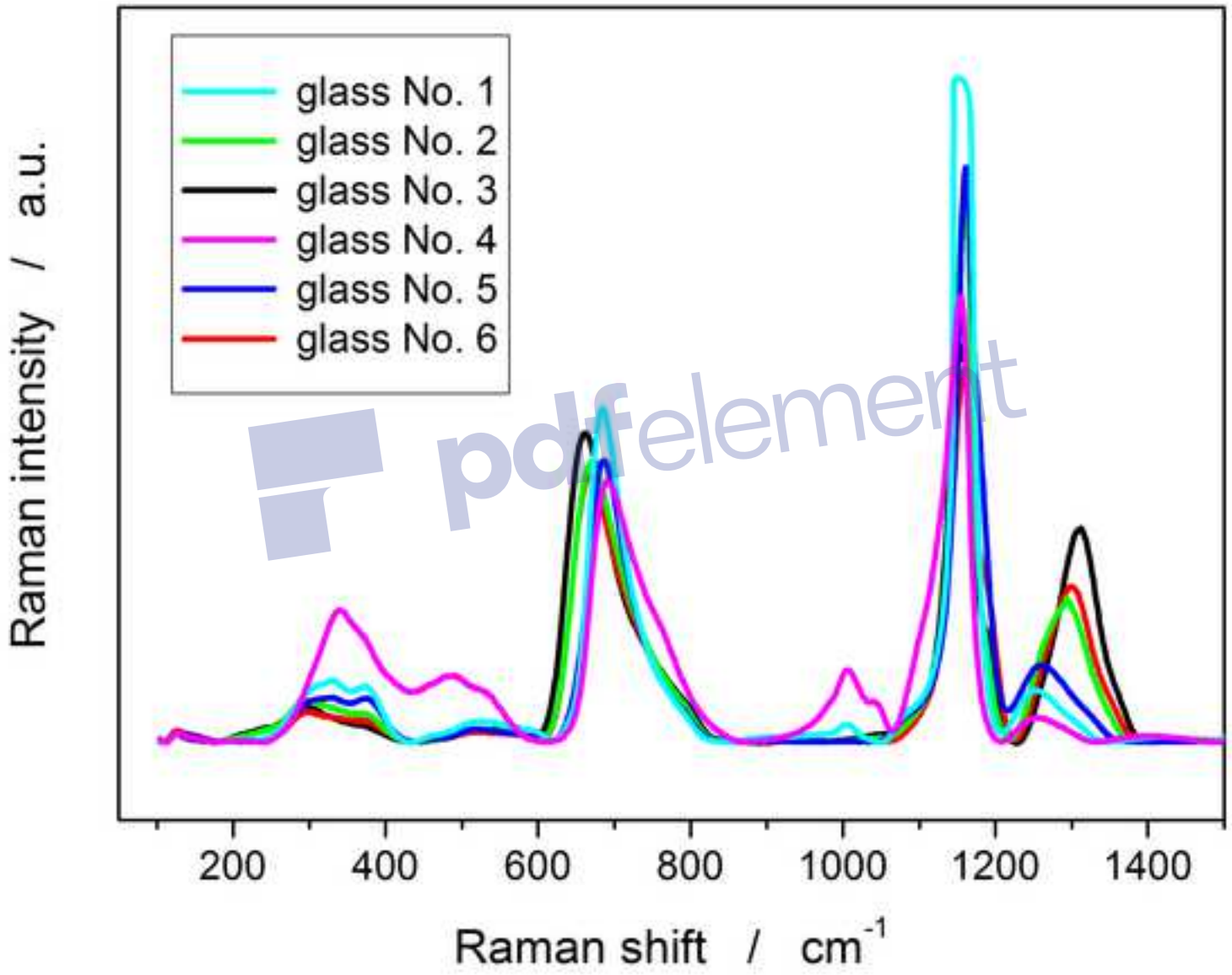

Figure 2

Click here to download high resolution image

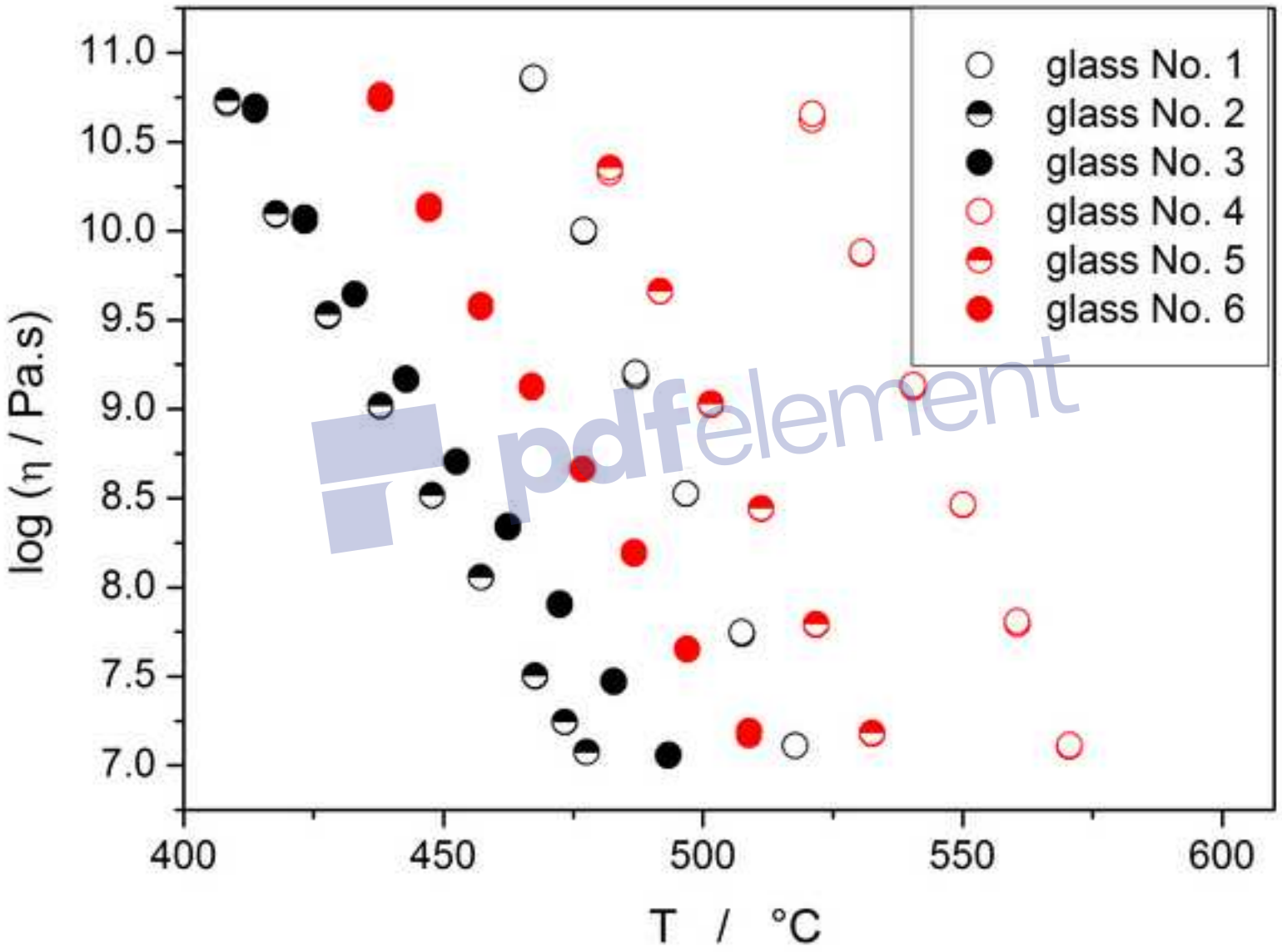

Figure 3

Click here to download high resolution image

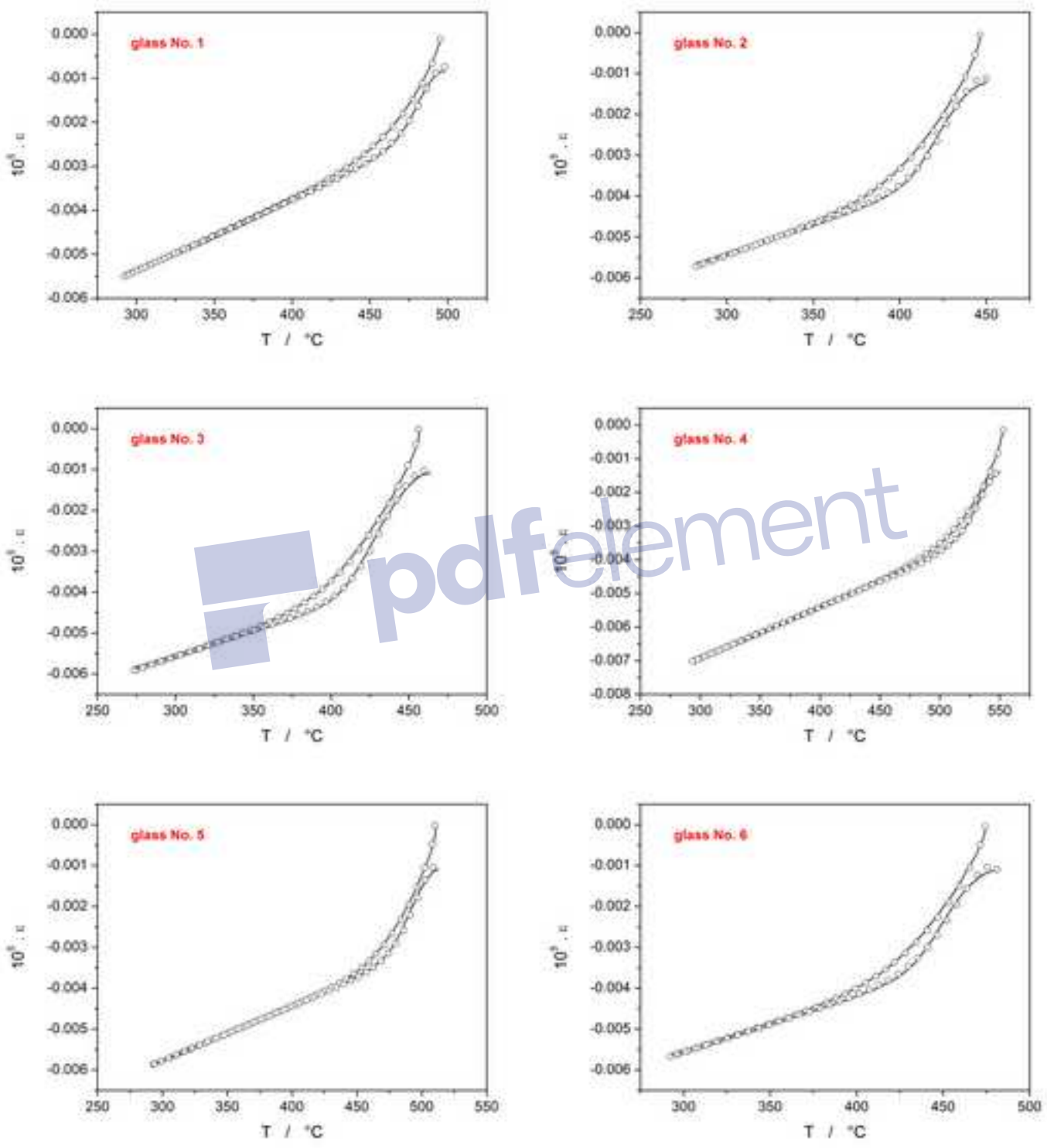

Figure 4

Click here to download high resolution image

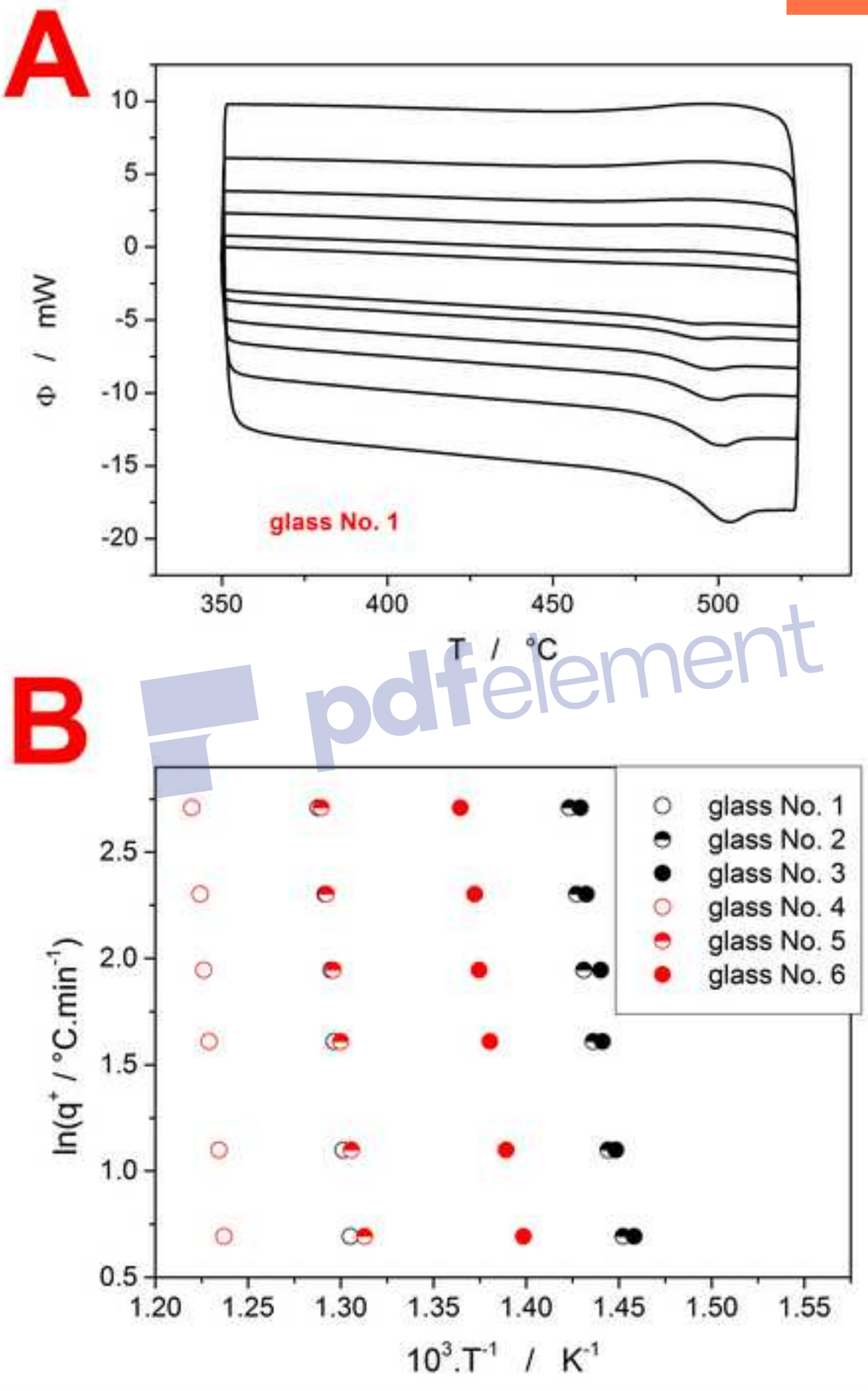

Figure 5

Click here to download high resolution image

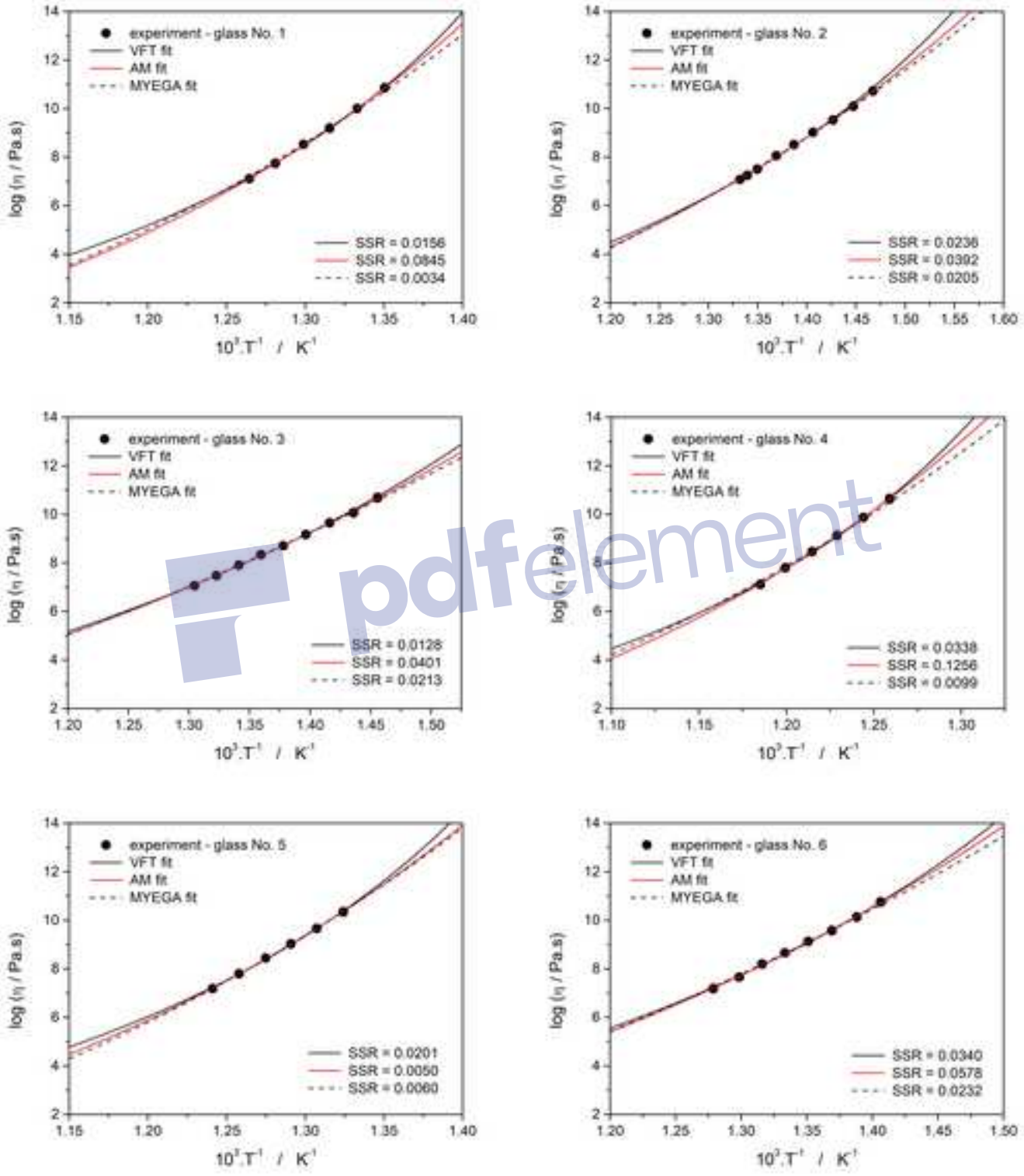

Figure 6

Click here to download high resolution image